symmetry

MDPI

Article

Spin-Dependent Scattering of Scalar and Vector Dark Matter on the Electron

Ke-Yun Wu * and Zhao-Hua Xiong

Faculty of Science, Beijing University of Technology, Beijing 100124, China; xiongzh@bjut.edu.cn
* Correspondence: keyunwu@emails.bjut.edu.cn

Abstract: The property of dark matter remains to date unknown. However, a model-independent classification of dark matter candidates can be achieved by using various symmetries, as performed in the standard model. Fermionic dark matter has been extensively researched, and one favored candidate is the neutralino in the Minimal Supersymmetric Standard Model, which is required by fermion–boson symmetry and the preservation of R-parity. Bosonic dark matter has not been sufficiently studied, especially the scenario of dark matter with a mass of sub-GeV. In this paper, we consider the effect of spin-dependent (SD) on scalar and vector dark matter, which are mediated by pseudoscalar and axial-vector, and evaluate the effect on the dark matter–electron scattering cross-section. We list all the interactions and form factor of dark matter–electron SD scattering, and use XENON10/100/1T experiment data to derive the exclusion limit of the SD cross-section. We find that the SD scattering of scalar and vector dark matter can be three orders of magnitude stronger than spin-independent (SI) scattering due to the *p*-wave scattering.

Keywords: spin-dependent scattering; scalar and vector; dark matter; electron

Citation: Wu, K.-Y.; Xiong, Z.-H. Spin-Dependent Scattering of Scalar and Vector Dark Matter on the Electron. *Symmetry* **2022**, *14*, 1061. https://doi.org/10.3390/sym14051061

Academic Editor: Roberto Passante

Received: 18 April 2022
Accepted: 18 May 2022
Published: 22 May 2022

1. Introduction

Approximately 27% of the energy density of our universe consists of dark matter which is non-luminous and rarely interacts with baryons [1]. Beyond gravitational phenomena, dark matter still has many elusive properties which include its mass and interactions. Usually, the methods of exploration for dark matter (DM) include direct detection, indirect detection, and collider experiments. Among all the candidates of dark matter, the most attractive one may be the weakly interacting massive particles (WIMPs). Among the candidates for dark matters, the lightest is Majorana fermion, i.e., neutralino in the Minimal Supersymmetric Standard Model, which is required by fermion–boson symmetry and the preservation of the global symmetry called R-parity. Clearly, prospects for the direct detection of dark matter crucially depend on whether WIMP–nucleon interactions are primarily spin-dependent or spin-independent. Although the property of dark matter remain unknown to date, one can perform a model-independent classification of dark matter candidates using symmetries. Firstly, WIMP dark matter is constrained to be neutral under both electromagnetism and color; secondly, if the WIMP-nucleon cross-section is primarily spin-dependent, scalar dark matter is disfavored; thirdly, the DM–nucleus interaction is described by an effective potential, which is a rotationally invariant scalar formed out of vectors: the relative velocity, DM position, and nuclear spin [2]. By using the effective potential and possible form of Lagrange, we can evolve the leading contributions to the cross-section.

Usually, the scattering of dark matter is divided into the SI and SD cases. SI scattering, which originated from the scalar couplings between dark matter and the target, dominates in detectors with a heavy nucleus. SD scattering, which originated from spin couplings, dominates in detectors with a light nucleus [3–9]. For SI scattering, the interaction will be mediated by a scalar or vector. The SD scattering can be modeled by setting the dark matter

which interacts solely with electron spin with a pseudoscalar or axial-vector mediator [10]. Then, p wave scattering always happens in SD scattering, and the exclusion limit of the corresponding cross-section can be enhanced by the momentum transfer [11]. This is a very different point compared with SI scattering. Furthermore, the SD limits of the fermionic dark matter were thoroughly studied in the literature [3,10]. However, the SD scattering of the scalar and vector dark matters still requires further study, especially the effects of the momentum transfer by the mediator.

Previous studies have mainly focused on DM with mass at the order of 100 GeV [12]. However, in recent dark matter detection, the limits of the WIMP cross-section approach the "neutrino floor" have become closer and closer, and less parameter space is left for detection. Instead, there is still a large space for the detection of light dark matter with a mass lighter than 1 GeV [13], due to the much smaller momentum transfer in the collision. Such light dark matter can scatter with electrons, causing the ionization of atoms in a detector target material and leading to single- or multi-electron events. We use 15 kg-days of data acquired in 2006 to set limits on the dark matter–electron scattering cross-section. As for the detection of the sub-GeV dark matter, the ionization signal will become more promising, since the electron recoil energies can exceed the threshold of the direct detection when the sub-GeV dark matter scatters on the electron [14–31]. Especially, in the dual-phase time projection chamber (TPC), the liquid XENON detector gives the most stringent constraint on the detection limits. When the dark matter particles scatter with the electron, the "S2" signal of the electron can be produced by electric fields upward into gaseous xenon in the liquid. The resulting recoil electrons have sufficient energy to ionize other atoms. The resulting signal includes the observed electron and scintillation photon.

In this work, scalar and vector types of dark matter are proposed and the corresponding effective operators are studied. The SD scattering of these dark matters, especially the effects of the momentum transfer, are numerically studied. The experiment data of XENON10, XENON100, and XENON1T [32–35] are used for numerical analysis. In SD scattering case, the spin of the electron will make the response function and form factors more complicated than the simple scalar interaction. Therefore, these form factor and response functions are calculated and the corresponding exclusion limit on the SD cross-sections are discussed.

The paper is organized as follows: the theoretical calculation of the cross-section and the benchmark model of the scalar and vector dark matter are shown in Section 2. In Section 3, we describe the recoil spectra and numerical results. The conclusion is given in Section 4.

2. The Dark Matter Model and the Form Factor

2.1. The Calculation Framework of Dark Matter and Electron Scattering Process

The scattering between the dark matter and the electrons is calculated under the impulse approximation in which the binding of the electrons is neglected. This approximation is a suitable method when the collision time is much shorter than the ionization of the target atom. Details of the condition and the comparison with the Born approximation can be found in [36–39]. As mentioned previously, the detailed calculations of the scattering are divided into the SI and SD cases. In case of the detection of the recoils of the nuclei, the rate of the SI case is proportional to the atomic number; thus, it is sensitive to heavy nuclei. However, the spin of nuclei is always considered to be coming from the single last unpaired nucleon; then, the detection will be relatively sensitive to the light nuclei. The calculation of the SD scattering on the nuclei is different from the SI case. For scattering on the electron, both the SI and SD cases are scattered on a single electron. Thus, at a first glance, all the scatterings should be taken into account as they seem to have the same weights from the theoretical side. What we can do in the simplest way is to consider couplings on the electron operators.

$$e^{\dagger}\boldsymbol{I}e, \;\; e^{\dagger}\boldsymbol{S}e. \tag{1}$$

The couplings to the first one can be seen as the cause of the SI scattering, while the couplings to the second one will cause SD scattering. The spin operator $\boldsymbol{S}$ is the non-relativistic limit of the quantum fermionic field which always comes from the γ matrices and then from the Dirac spin

$$\boldsymbol{\sigma}^s = 2\boldsymbol{S}, \tag{2}$$

with

$$\boldsymbol{\sigma}^s = \gamma^0\boldsymbol{\gamma} = \begin{pmatrix} \boldsymbol{\sigma} & 0 \\ 0 & \boldsymbol{\sigma} \end{pmatrix}. \tag{3}$$

In general, the spin operators originate from a pseudoscalar or an axial-vector mediator. Both SI and SD scattering can be considered in a uniform formula which will be subsequently discussed.

In the direct detection, the measured quantity is the counting rate R^{ion} which is theoretically predicted by the velocity-averaged cross-section between dark matter and the target. In the direct detection, the differential event rate that is induced by ionizing electron can be written as

$$\begin{aligned} \frac{dR^{\text{ion}}}{dE_R} &= N\frac{\rho_\chi}{m_\chi}\frac{\bar{\sigma}_e}{8\mu_{\chi e}^2} \\ &\quad \times \int qdq|F_{\text{DM}}(q)|^2\mathcal{R}_{(\text{ion})}(E_R,q)\eta(v_{\min}). \end{aligned} \tag{4}$$

in which $\rho_\chi = 0.4\,\text{GeV/cm}^3$ is the local dark matter density and the number of target atoms is N. E_R and q are the recoil energy and momentum transfer of the electron, respectively. $\bar{\sigma}_e$ is the reduced cross-section and $\mu_{\chi e} = m_\chi m_e/(m_\chi + m_e)$ is the reduced mass of dark matter (m_χ) and electron (m_e).

In Equation (4), we apply the response function $\mathcal{R}_{(\text{ion})}$ to denote the wave function of electron ionization $|f_{\text{ion}}^{nl}|^2$ [40,41]. Compared with SI scattering, the interaction in SD scattering will consider the spin operator of the electron which comes from the Dirac spin $\boldsymbol{\sigma}^s$. Thus, in this case, the wave function of the electron is not plane wave $e^{i\boldsymbol{q}\cdot\boldsymbol{r}}$ but is a more complex form $e^{i\boldsymbol{q}\cdot\boldsymbol{r}}\boldsymbol{\sigma}^s$. We follow Refs. [11,42] to write these two functions as

$$\begin{aligned} \mathcal{R}_{\text{SI}}^{\text{ion}}(E_R,q) &= \sum_{J_f}\overline{\sum_{J_i}}\left|\langle J_f|\sum_{i=1}^{Z}e^{i\boldsymbol{q}\cdot\boldsymbol{r}_i}|J_i\rangle\right|^2 \\ &\quad \times\delta(E_{J_f} - E_{J_i} - E_R) \end{aligned} \tag{5}$$

and

$$\begin{aligned} \mathcal{R}_{\text{SD}}^{\text{ion}}(E_R,q) &= \sum_{J_f}\overline{\sum_{J_i}}\sum_{k}\left|\langle J_f|\sum_{i=1}^{Z}e^{i\boldsymbol{q}\cdot\boldsymbol{r}_i}\sigma_{i,k}^s|J_i\rangle\right|^2 \\ &\quad \times\delta(E_{J_f} - E_{J_i} - E_R). \end{aligned} \tag{6}$$

in which the $\langle J_f|\cdots|J_i\rangle$ is the transition amplitude from the initial state $|J_i\rangle$ to the final state $\langle J_f|$. $\sigma_{i,k}^s$ is Dirac spin. The delta function imposes the energy conservation of the

transition. The summations all the electrons at different shells gives the response functions. The ratio r of the SD and SI response function is given by (see Refs. [11,40,43])

$$r = \frac{\mathcal{R}_{\rm SD}^{\rm ion}}{\mathcal{R}_{\rm SI}^{\rm ion}} = 3. \tag{7}$$

The ratio $r = 3$ is because the dependence on the recoil energy E_R can be ignored when the recoil energy is less than 0.2 keV, as shown in Ref. [11].

The $\eta(v_{min})$ which is the velocity distribution of dark matter follow Maxwell–Boltzmann. In the calculation, we assume that the incoming velocity of dark matter is $\boldsymbol{v}$, and the outgoing momentum of dark matter and electron are $\boldsymbol{p}'_\chi$ and $m_e \boldsymbol{v}_e$. Therefore, the momentum conservation is given by

$$\boldsymbol{q} = m_\chi \boldsymbol{v} - \boldsymbol{p}'_\chi = m_e \boldsymbol{v}_e \tag{8}$$

and the energy conservation is given by

$$\Delta E_e = \frac{1}{2} m_\chi v^2 - \frac{|m_\chi v - q|^2}{2 m_\chi} = \boldsymbol{v} \cdot \boldsymbol{q} - \frac{\boldsymbol{q}^2}{2 m_\chi}, \tag{9}$$

where $\Delta E_e = E_{\rm b} + E_R$ is the transferred energy which is dependent on the binding energy $E_{\rm b}$ and recoiled energy E_R. From Equation (9), the minimum velocity $v_{\rm min}$ required for ionizing the electron in the (n, l) shell is given by

$$v_{\rm min} = \frac{|E_{\rm b}^{nl}| + E_R}{q} + \frac{q}{2 m_\chi}. \tag{10}$$

As such, the Maxwell–Boltzmann velocity distribution for the minimum velocity $\eta(v_{\rm min})$ can be given by

$$\eta(v_{\rm min}) = \int_{v_{\rm min}} \frac{d^3 v}{v} f_\chi(v) \Theta(v - v_{\rm min}), \tag{11}$$

with

$$f_\chi(\vec{v}_\chi) \propto e^{-\frac{|\vec{v}_\chi + \vec{v}_E|^2}{v_0^2}} \Theta(v_{\rm esc} - |\vec{v}_\chi + \vec{v}_E|), \tag{12}$$

in which we assume that the circular velocity $v_0 = 220$ km/s, cut at the escaping velocity $v_{\rm esc} \sim 544$ km/s and the averaged Earth relative velocity $v_E = 232$ km/s [44,45].

Finally, we discuss the scattering cross-section σ_e between the dark matter and electron from Equation (4). In order to study the effect of momentum transfer, the reduced cross-section $\bar{\sigma}_e$ and momentum-dependent factor $F_{\rm DM}(q)$ are introduced. The scattering cross-section can be written as

$$\sigma_e = \bar{\sigma}_e |F_{\rm DM}|^2, \tag{13}$$

in which $\bar{\sigma}_e$ is a reduced cross-section with momentum independence. It is given by

$$\bar{\sigma}_e = \mu_{\chi e}^2 \frac{\overline{|M(q = q_0)|^2}}{16 \pi m_\chi^2 m_e^2}, \tag{14}$$

Then, the form factor $F_{\rm DM}(q)$ is given by [46]

$$|F_{\rm DM}(q)|^2 = \frac{\overline{|M(q)|^2}}{|M(q = q_0)|^2}, \tag{15}$$

where $q_0 = \alpha m_e$ is the reference momentum. We can see that all the effect of the momentum transfer is absorbed in the form factor from Equation (15). In Ref. [27], the form factor is considered as 1 and $1/q^2$ for the heavy and light mediator in SI scattering. However, in SD scattering, the form factor is more complicated and dependent on the momentum transfer due to the appearance of γ_5 in the mediator. All the form factors of the scalar and vector dark matter are discussed in the next subsection.

2.2. Benchmark Model of Scalar and Vector Dark Matter

In order to check the effect of the momentum transfer in SD scattering, the scalar dark matter with scalar the mediator is studied in our numerical calculations. The interaction can be simplified as

$$\mathcal{L}_{\rm int} = a g_\chi \phi^2 + a g_e \bar{e} \gamma_5 e, \tag{16}$$

in which g_χ and g_e is the coupling constant of the dark matter and electron, respectively. The scalar dark matter and electron are characterized by ϕ and e, respectively. The scalar mediator is denoted by a. With Equation (16), we can obtain the momentum dependent form factor $F_{\rm DM}$ from Equation (15)

$$|F_{\rm DM}|^2 = \frac{q^2(m_a^2 + q_0^2)^2}{q_0^2(m_a^2 + q^2)^2}, \tag{17}$$

where m_a (m_χ) is the mass of the mediator (dark matter). q_0 and q are the reference and momentum transfer, respectively. The details can be found in Appendix A. In order to fully reflect the effect of the momentum transfer, the interaction with the vector dark matter is also considered. We listed all the interactions [2] between the scalar (ϕ) and vector (B) dark matter and the electron with pseudoscalar (a) and axial-vector (A) mediator in Table 1. The scattering amplitudes is listed in Appendix A. To compare with SI scattering, the corresponding form factor and the approximation in the massive and massless form factor are also listed in the table. We can see when the mass of the mediator is massive or massless, the form factor is approximately equal to 1, q^2 or $1/q^2$, thus yielding results which show the limits to be very simple as well as similar. However, in fact, the form factors have a much more analytically complicated q dependence, as can be seen from Table 1.

These form factors are plotted in the top of Figure 1 to explore the effect of the momentum transfer on SD scattering. For comparison, we also plotted the SI form factor with the scalar or vector mediator for the scalar dark matter in the bottom panel. The effect of the momentum transfer is discussed in next section.

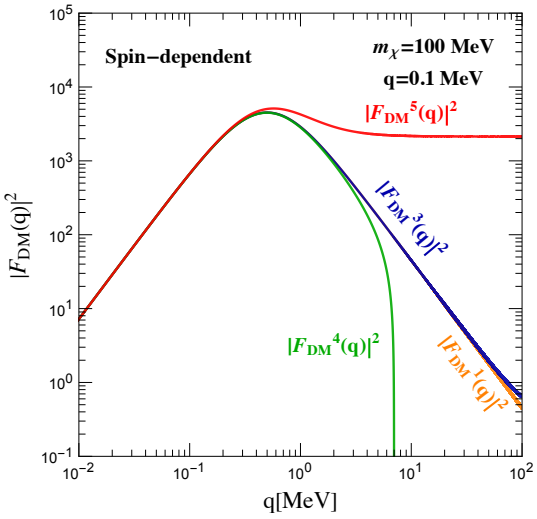

Figure 1. *Cont.*

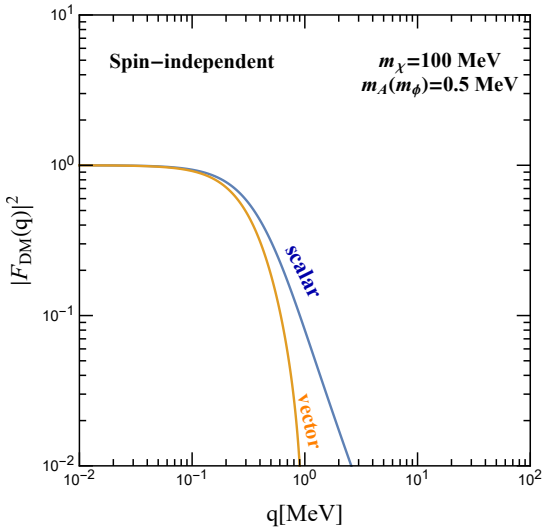

Figure 1. Top panel: the form factor $|F_{\rm DM}(q)|$ for the SD scattering of the scalar and vector dark matter with pseudoscalar or axial-vector mediator. Bottom panel: the form factor $|F_{\rm DM}(q)|$ for the SI scattering of the fermionic dark matter with a scalar or vector mediator. $m_\chi = 100$ MeV for each panel.

Table 1. Different operators which induce the spin-dependent scattering between the dark matter and the electron. To compare with SI scattering, the corresponding form factor and the approximation in the massive and massless form factors are also listed.

DM Coupling	Electron Coupling	$\lvert F_{\rm DM}(q)\rvert^2$	Massive	Massless
$ag_\chi\phi^2$	$ag_e\bar{e}\gamma_5 e$	$\lvert F^1_{\rm DM}\rvert^2 = \frac{q^2(m_a^2+q_0^2)^2}{q_0^2(m_a^2+q^2)^2}$	$\approx\frac{q^2}{q_0^2}$	$\approx\frac{q_0^2}{q^2}$
$g_\chi(\phi^\dagger\partial_\mu\phi-\phi\partial_\mu\phi^\dagger)A^\mu$	$g_e\bar{e}\gamma_\mu\gamma_5 eA^\mu$	$\lvert F^2_{\rm DM}\rvert^2 = \frac{q^2(m_A^2+q_0^2)^2}{q_0^2(m_A^2+q^2)^2}$	$\approx\frac{q^2}{q_0^2}$	$\approx\frac{q_0^2}{q^2}$
$ag_\chi B_\mu B^\mu$	$ag_e\bar{e}\gamma_5 e$	$\lvert F^3_{\rm DM}\rvert^2 = \frac{q^2(m_a^2+q_0^2)^2(4m_\chi^2q^2+12m_\chi^4+q^4)}{q_0^2(m_a^2+q^2)^2(4m_\chi^2q_0^2+12m_\chi^4+q_0^4)}$	$\approx\frac{q^2}{q_0^2}$	$\approx\frac{q_0^2}{q^2}$
$g_\chi B^\dagger_\nu\partial_\mu B^\nu A^\mu$	$g_e\bar{e}\gamma_\mu\gamma_5 eA^\mu$	$\lvert F^4_{\rm DM}\rvert^2 = \frac{q^2(m_A^2+q_0^2)^2(4m_\chi^2q^2+12m_\chi^4+q^4)}{q_0^2(m_A^2+q^2)^2(4m_\chi^2q_0^2+12m_\chi^4+q_0^4)} \times\frac{(m_A^2m_\chi-m_eq^2)(2m_A^2m_e+m_A^2m_\chi+m_eq^2)}{(m_A^2m_\chi-m_eq_0^2)(2m_A^2m_e+m_A^2m_\chi+m_eq_0^2)}$	$\approx\frac{q^2}{q_0^2}$	1
$g_\chi B_\mu\partial^\mu B_\nu A^\nu$	$g_e\bar{e}\gamma_\mu\gamma_5 eA^\mu$	$\lvert F^5_{\rm DM}\rvert^2 = \frac{q^2(m_A^2+q_0^2)^2}{q_0^2(m_A^2+q^2)^2} \times\frac{-16m_e^2m_\chi^4-2m_\chi^2q^2(m_e-m_\chi)^2+m_e^2q^4+2m_em_\chi q^4}{-16m_e^2m_\chi^4-2m_\chi^2q_0^2(m_e-m_\chi)^2+m_e^2q_0^4+2m_em_\chi q^{04}}$	$\approx\frac{q^2}{q_0^2}$	$\approx\frac{q_0^2}{q^2}$

3. Recoil Spectra and Numerical Results

3.1. The Procedure of Numerical Simulations

We follow the procedure described in Ref. [26] to calculate the constraints in the experimental data. The total quantum number which can be produced by electron recoil energy $E_{\rm R}$ induces the observed electron n_e and scintillation photons n_γ. $n^{(1)} = \text{Floor}\ (E_{\rm R}/W)$ in which the $W = 13.8$ eV is the minimum energy to produce a quantum number. We choose $f_R = 0$, $f_e = 0.83$ as the fiducial values. The uncertainty is defined as $0 < f_R < 0.2$, $12.4 < W < 16$ eV, and $0.62 < f_e < 0.91$. In our work, we mainly consider the shells of the electron as $(5s,\ 4d,\ 4p,\ 4s)$ which have energies of $(13.3,\ 63.2,\ 87.9,\ 201.4)$ eV. There are

also many additional quanta numbers in these shells under the effect of photoionization. The additional quanta numbers in shell $(5s,\ 4d,\ 4p,\ 4s)$ are $(0,\ 4,\ 6\text{–}10,\ 3\text{–}15)$, respectively, Ref. [27]. These quanta numbers also include the observed electron n_e and scintillation photons n_γ. All the quanta number is $(n^1 + n^2)$ which obeys a binomial distribution. We can obtain the number of electrons n_e by calculating the corresponding distributions. These additional quanta numbers, binding energy of electron, and photon energy are listed in the Table 2 [27,47].

Table 2. The number of additional quanta and binding energy from the Xenon $(5p^6,\ 5s^2,\ 4d^{10},\ 4p^6,\ 4s^2)$ shells.

Shell	$5p^6$	$5s^2$	$4d^{10}$	$4p^6$	$4s^2$
Binding Energy (eV)	12.6	25.7	75.6	163.5	213.8
Photon Energy (eV)	-	13.3	63.2	87.9	201.4
Additional Quanta	0	0	4	6–10	3–15

On the experimental side, the weak signal of the electron cannot be observed. In order to measure the amount of electrons n_e, we must amplify the electron signal by the photomultiplier tuber. The signal of the electron is converted to the photo-electrons (PEs). We apply the experimental data from XENON10 data [26] (15 kg–days), XENON100 data [32,34] (30 kg–years) and XENON1T data [35] (1.5 tones–years) to compare our theory result. The boundary limits of the SD scattering cross-section are obtained by comparing these results. The number of PE and n_e obey Gaussian distribution. The PE can be produced by calculating this Gaussian function which has a mean $n_e\mu$ and width $\sqrt{n_e}\sigma$, in which $\mu = 27\ (19.7, 11.4)$ and $\sigma = 6.7\ (6.2, 2.8)$ for XENON10 (XENON100, XENON1T). We follow Refs. [26,32,35] to obtain the PE bins. Note that in our numerical evaluation, the range of the PE bin in the XENON1T is only chosen as [165, 275].

For SI scattering, the form factor will be suppressed by the momentum transfer in the light mediator from the literature [26]. However, for SD interaction, the form factors are more complicated in Equation (17) and Table 1. To explore the effect of the momentum transfer on SD scattering, the spectra of the electron from $F_{\rm DM} = 1$ (top) and $F^1_{\rm DM}(q)$ (bottom) are plotted in Figure 2. Herein, the mediator m_a is set as 0.5 MeV and the fiducial cross-section $\bar{\sigma}_e$ is set as 5×10^{-39} cm^2. We choose the masses of dark matter as $m_\chi = 10$ MeV, 30 MeV, 100 MeV, 300 MeV for comparison, and the exposure is set as 1000 kg–yr. From Figure 2, it can be seen that the number of the electron is the same in the same dark matter mass. This is because the quantum number depends on the recoil energy E_R which can be produced by the incoming energy of dark matter $(1/2m_\chi v^2)$. However, the event rates of the $F^1_{\rm DM}(q)$ (bottom) can always be enhanced by two orders of magnitude greater than $F_{\rm DM} = 1$ for all masses of dark matter. We understand this result from Equation (4). This shows that the event rates will depend on the form factor $F_{\rm DM}$. This implies that the momentum transfer plays an important role in the dark matter form factor.

The dependence of the SD form factor on the momentum transfer is shown in the left panel of Figure 1. Herein, all the form factors from Table 1 are considered. The mass of the dark matter is set to $m_\chi = 100\,$MeV and the mass of the mediator is chosen as $m_A(m_\phi) = 0.5\,$MeV. In order to explore the difference between SD scattering and SI scattering in the form factor with the light mediator, we also plotted the form factor of SI in the bottom panel. We can see that most form factors of SD scattering are greater than SI scattering. Furthermore, the maximum value of the SD form factor can be four orders of magnitude stronger than $F_{\rm DM} = 1$. The SD form factor can be the maximum value when the momentum transfer q is approximately equal to mediator mass. For different interactions, the form factor can be the difference, so the form factor is model dependent. We find that the mass of the mediator also affects the value of the form factor in Equation (17). Therefore, we plot the dependence of the SD form factor on the mass of mediator in Figure 3. We can see the form factor will not change when $m_a(m_A)$ is greater than 0.1 MeV in Figure 3. However,

for a light mediator, the form factor will be suppressed by the mass of the mediator. The mediator therefore also plays an important role in the form factor. Therefore, we set the mass of the mediator to 0.5 MeV to show the effect of momentum transfer.

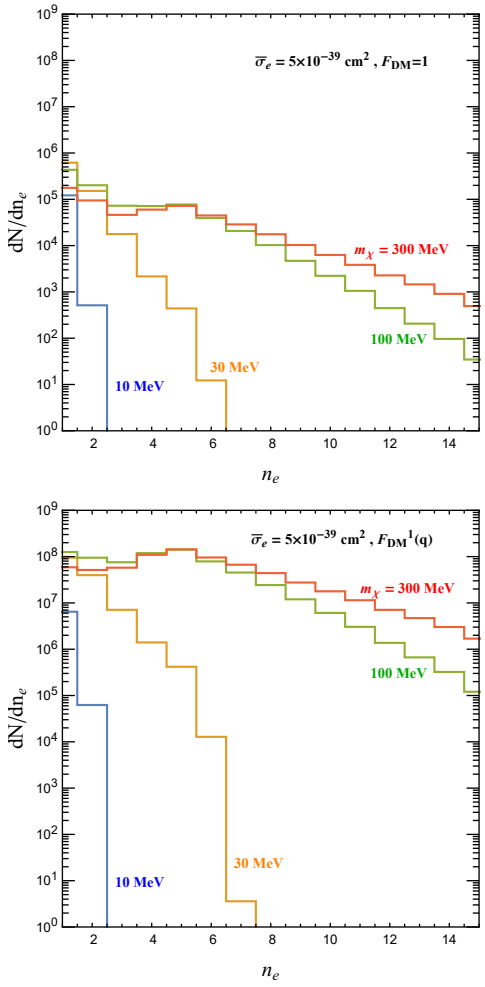

Figure 2. The spectra of the electron from the scalar dark matter scattering with the electron in $F_{\rm DM} = 1$ (**top**) and $F^1_{\rm DM}(q)$ (**bottom**). We choose $m_\chi = 10$ MeV (blue), 30 MeV (orange), 100 MeV (green) and 300 MeV (red) for comparison. Furthermore, the fiducial cross-section and exposure were chosen as $\bar{\sigma}_e = 5 \times 10^{-39}{\rm cm}^2$ and 1000 kg–yr.

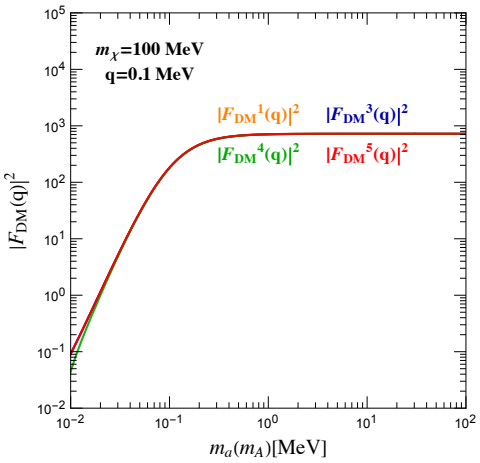

Figure 3. The relation between the form factor $|F_{\rm DM}(q)|$ and the different mass of mediator. Herein, the momentum transfer q is set to 0.1 MeV and the mass of dark matter is chosen as 100 MeV.

3.2. The Result and Analysis of Numerical Simulations

As we discussed above, in the light mediator, the SD and SI form factors can be suppressed by momentum transfer. This result satisfies the long-range interaction. Furthermore, it can also be enhanced by the mass of the mediator. However, in a heavy mediator, the SI form factor will be constant 1, which is called the contact interaction. The SD form factor can be enhanced by momentum transfer. The reason for this result is that the SD and SI scattering are p-wave scattering and s-wave scattering, respectively. Additionally, when we define the reduced cross-section $\bar{\sigma}_e$ in the specific momentum q_0, the corresponding form factors are always proportional to the momentum transfer. The different q_0 can make the reduced cross-section $\bar{\sigma}_e$ and form factor change greatly. Thus, the definition points q_0 are also more important in the SD scattering. The specific form factor $F_{\mathrm{DM}}(q)$ can be seen from Table 1 and the numerical results in Figure 1.

In order to explore the limits of SD scattering and we plotted the dependence of the SD reduced cross-section $\bar{\sigma}_e$ on the mass of dark matter in Figure 4. From Equation (4), we can see that the reduced cross-section $\bar{\sigma}_e$ will decrease as the form factor F_{DM} increases when the counting rate R is a constant value. In Figure 4, we use the dotted line and shades to show the result of $F_{\mathrm{DM}} = 1$ and $F_{\mathrm{DM}}(q)$, respectively. The orange area, blue area and red area denote XENON10 data, XENON100 data and XENON1T data, respectively. The top picture of Figure 4 is the result of the pseudoscalar mediator. The upper left represents the scalar dark matter $(F^1_{\mathrm{DM}}(q))$ and the right one is the vector dark matter$(F^3_{\mathrm{DM}}(q))$. The bottom picture of Figure 4 is the result of the axial-vector mediator of the vector dark matter in axial-vector mediator $(F^4_{\mathrm{DM}}(q), F^5_{\mathrm{DM}}(q))$. Compared with $F_{\mathrm{DM}} = 1$ (dotted line), we can see that the cross-section on SD scattering will be significantly enhanced. This is because the form factor can be enhanced as the momentum transfer improves. The improved form factor can affect the reduced cross-section from Equation (13). We also found that the exclusion limits of the SD scattering cross-section are more sensitive in the region of $m_\chi > 100$ MeV. It can be understood from Figure 2, in which the range of electron n_e is very small in light dark matter ($m_\chi < 100$ MeV). When $m_\chi > 100$ MeV, the range of the electron and the event can be the largest, but the range of the electron does not change and the event can be reduced when $m_\chi > 300$ MeV.

In the above calculation, we set the mass of the mediator m_a (m_A) as 0.5 MeV. This is because, in this case, the form factor can become the maximum value. Here, the momentum transfer q is approximately equal to the mass of the mediator from Figure 1. We also found that the form factor will depend on the mass of the mediator from Figure 3. The definition of q_0 and the mass of the mediator can affect the form factor and reduced cross-section. Thus, we show all the exclusion limits in $q_0 = \alpha m_e$ and $m_A(m_a) = 0.5$ MeV for the comparisons between the different models. The results are plotted in Figure 4. Furthermore, we can obtain the following conclusions.

1. The q_0 must be defined at a specific value αm_e to compare the reduced cross-section $\bar{\sigma}_e$ of SD and SI scattering. In this scene, the reduced cross-section of the SD scattering can be three orders of magnitude large than the SI scattering due to the effect of transferred momentum.
2. The form factor $F^1_{\mathrm{DM}}(q)$, $F^2_{\mathrm{DM}}(q)$, $F^4_{\mathrm{DM}}(q)$ and $F^5_{\mathrm{DM}}(q)$ can recover Λ^2/q^2 and the F^3_{DM} can recover 1 in massless mediator. From this result, we can know that the form factors of SD can recover the SI in the vanishing mediator mass. All the form factor is proportional to q^2 in the heavy dark matter which can enhance the exclusion limits.

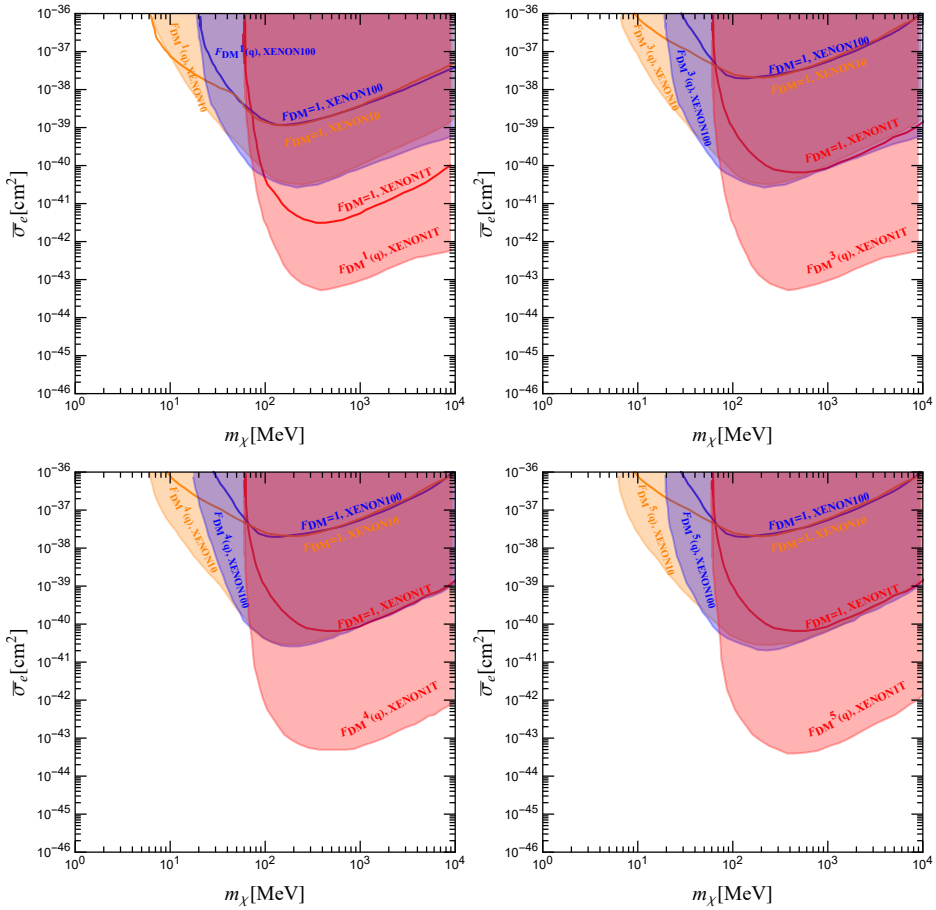

Figure 4. The limits on Bosonic dark matter–electron with pseudoscalar mediator (**top panel**) and axial-vector mediator (**bottom panel**), respectively. Furthermore, results for the scatter and vector dark matters are displayed in the left panel and right panel. These limits are from XENON1T (red), XENON100 (blue) and XENON10 (orange) data. The $F_{\rm DM}^1 = F_{\rm DM}^2$, so they have the same limits of the scattering cross-section (**upper left**). The corresponding results from $F_{\rm DM} = 1$ (line) are also shown in each panel for the comparison.

4. Conclusions

The experiment efforts to search for the dark matter–electron coupling motivate the consideration of the scalar and vector dark matter candidate. In this paper, we calculate all the form factor from the dark matter–electron couplings mediated by the pseudoscalar and axial-vector. We also plotted the dependence on the mass of the dark matter of the SI and SD reduced cross-section.

Our result show that the form factor of SD scattering can be four orders of magnitude larger than SI scattering when the momentum transfer is less than the mass of the mediator $(q < 0.5\ \text{MeV})$. For the light mediator $(q > 0.5\ \text{MeV})$, the form factor will be suppressed in SI and SD scattering. Due to the peak value of SD scattering being much greater than 1, the SD scattering form factor will be greater than SI scattering. The exclusion limits of the SD scattering cross-section which are dependent on the form factor will also be enhanced in the light mediator. It can be 10^{-44} cm^2 in XENON1T. This result is the same as the fermion dark matter from the literature [11]. The reason for this result is that the SD scattering is p-wave scattering. We also find that the form factor is not affected by the mediator when the mass of the mediator is greater than the momentum transfer. However, when $m_a < 0.1$ MeV, the form factor will be improved as the mass of the mediator increases.

Author Contributions: Conceptualization, K.-Y.W. and Z.-H.X.; methodology, K.-Y.W.; software, K.-Y.W.; validation, K.-Y.W. and Z.-H.X.; formal analysis, K.-Y.W. and Z.-H.X.; investigation, K.-Y.W.; resources, K.-Y.W.; data curation, K.-Y.W.; writing—original draft preparation, K.-Y.W.; writing—review and editing, Z.-H.X.; visualization, Z.-H.X.; supervision, Z.-H.X.; project administration, K.-Y.W. and Z.-H.X. All authors have read and agreed to the published version of the manuscript.

Funding: This research was funded by the Natural Science Foundation of China under grant number 11775012.

Acknowledgments: This work was supported by the Natural Science Foundation of China under grant number 11775012. We would like to thank Bin Zhu and Wulong Xu for many useful discussions on SD theory and for procedural guidance. The authors are also grateful to Lei Wu, Liangliang Su and Aichen Li for many useful discussions on the form factor and the effect of transferring momentum.

Conflicts of Interest: The authors declare no conflict of interest.

Appendix A. DM Form Factor and Scattering Amplitudes

For a scalar DM with a pseudoscalar mediator, the interaction can be written as

$$\mathcal{L}^1_{\rm int} = a g_\chi \phi^2 + a g_e \bar{e}\gamma_5 e. \tag{A1}$$

The scattering amplitude is given by

$$M = \frac{g_\chi}{q^2 - m_a^2}\bar{U}_e(p_2)(i g_e \gamma_5) U_e(p_4), \tag{A2}$$

in which we assume that the incoming momentum of the dark matter and electron are p_1 and p_2, respectively. The outgoing momentum of the dark matter and electron are p_3 and p_4, respectively. The q is momentum transfer. The $|M|^2$ can be obtained by summing the spin.

$$\Sigma_{spin}\overline{|M|^2} = \frac{g_\chi^2 g_e^2}{(q^2 - m_a^2)^2}\Big(\bar{U}_e(p_2)\gamma_5 U_e(p_4)\Big)\Big(\bar{U}_e(p_4)\gamma_5 U_e(p_2)\Big) \tag{A3}$$

$$= \frac{g_\chi^2 g_e^2}{(q^2 - m_a^2)^2}\Big(tr\Big[(p_4^l\gamma_l + m_e)\gamma_5(p_2^m\gamma_m + m_e)\gamma_5\Big]\Big). \tag{A4}$$

Wherein the result of trace is given by

$$tr[(p_4^l\gamma_l + m_e)\gamma_5(p_2^m\gamma_m + m_e)\gamma_5] \tag{A5}$$

$$= -4p_4 \cdot p_2 + 4m_e^2. \tag{A6}$$

Thus, the amplitude square is

$$\Sigma_{spin}\overline{|M|^2} = \frac{4 g_\chi^2 g_e^2}{(q^2 - m_a^2)^2}(-p_4 \cdot p_2 + m_e^2), \tag{A7}$$

The effect of momentum p_2 and p_4 can be offset by Mandelstam variables s, t, u. Herein, $s = (p_1 - p_2)^2$, $t = (p_1 - p_3)^2$, $u = (p_1 - p_4)^2$. Furthermore, we assume the electron to be at rest, and the incoming momentum can be written as:

$$p_1 = (m_\chi, 0, 0, p), \qquad p_2 = (m_e, 0, 0, 0), \tag{A8}$$

$$p_3 = (m_\chi - E_R, p_{31}, p_{32}, p_{33}),\ p_4 = (m_e + E_R, p_{41}, p_{42}, p_{43}). \tag{A9}$$

wherein the E_R is the recoil energy. The s, t, u can be expressed by m_e and m_χ

$$\begin{cases} s = (m_\chi + m_e)^2 \\ t = -2m_e E_R \\ u = (m_e - m_\chi)^2 + 2E_R m_e. \end{cases} \tag{A10}$$

Applying the Mandelstam variables, the $\overline{|M|^2}$ is given by

$$\overline{|M|^2} = \frac{-2tg_\chi^2 g_e^2}{(m_a^2 - t)^2} = \frac{4m_e E_R g_\chi^2 g_e^2}{(m_a^2 + 2m_e E_R)^2} = \frac{2q^2 g_\chi^2 g_e^2}{(m_a^2 + q^2)}. \tag{A11}$$

where we apply equation $q^2 = 2m_e E_R$. In order to explore the effect of the momentum transfer, the reduced amplitude $\overline{|M(q_0)|^2}$ and momentum-dependent factor $F_{\mathrm{DM}}(q)$ are introduced. The $\overline{|M|^2}$ can be written as

$$\overline{|M|^2} = \overline{|M(q_0)|^2} \times |F_{\mathrm{DM}}(q)|^2, \tag{A12}$$

we choose the $q_0 = \alpha m_e$ as reduced momentum. In this case, the $\overline{|M(q_0)|^2}$ is given by

$$\overline{|M(q_0)|^2} = \frac{2g_\chi^2 g_e^2 (\alpha m_e)}{(m_a^2 + (\alpha m_e)^2)^2}. \tag{A13}$$

The DM form factor $F_{\mathrm{DM}}(q)$ can be obtained from Equation (A12)

$$F_{\mathrm{DM}} = \frac{q^2(m_a^2 + q_0^2)}{q_0^2(m_a^2 + q^2)} = \frac{q^2(m_a^2 + (\alpha m_e)^2)}{(\alpha m_e)^2(m_a^2 + q^2)}. \tag{A14}$$

As such, when the mediator is the axial-vector with the interaction

$$\mathcal{L}_{\mathrm{int}}^2 = g_\chi(\phi^\dagger \partial_\mu \phi - \phi \partial_\mu \phi^\dagger) A^\mu + g_e \bar{e} \gamma_\mu \gamma_5 e A^\mu, \tag{A15}$$

The scattering amplitude is given by

$$\overline{|M|^2} = -\frac{16 E_R g_e^2 g_\chi^2 m_e (m_e + m_\chi)^2}{(2E_R m_e + m_A^2)^2}. \tag{A16}$$

For vector DM with a pseudoscalar mediator, the interaction and scattering amplitude are

$$\mathcal{L}_{\mathrm{int}}^3 = a(g_\chi B_\mu B^\mu + g_e \bar{e} \gamma_5 e) \tag{A17}$$

and

$$\overline{|M|^2} = \frac{2E_R g_e^2 g_B^2 m_e (4E_R^2 m_e^2 + 8E_R m_e m_\chi^2 + 12 m_\chi^4)}{3m_\chi^2 (2E_R m_e + m_a^2)^2}. \tag{A18}$$

When the mediator is an axial-vector, the interaction and scattering amplitudes are

$$\mathcal{L}_{\mathrm{int}}^4 = g_\chi B_\nu^\dagger \partial_\mu B^\nu A^\mu + g_e \bar{e} \gamma_\mu \gamma_5 e A^\mu \tag{A19}$$

and

$$\overline{|M|^2} = \frac{2E_R g_e^2 g_\chi^2 m_e (E_R^2 + 2E_R m_e m_\chi + 3m_\chi^4)(4E_R^2 m_e^4 + 4E_R m_e^3 m_A^2 - m_A^4 m_\chi (2m_e + m_\chi))}{3m_A^4 m_\chi^4 (2E_R m_e + m_A^2)^2}. \tag{A20}$$

Furthermore, the other interaction with the axial-vector is

$$\mathcal{L}_{\mathrm{int}}^5 = g_\chi B_\mu \partial^\mu B_\nu A^\nu + g_e \bar{e} \gamma_\mu \gamma_5 e A^\mu \tag{A21}$$

and

$$\overline{|M|^2} = -\frac{8E_R g_e^2 g_\chi^2 m_e^2 [E_R^2 m_e^2 (m_e + 2m_\chi) - E_R m_\chi^2 (m_e - m_\chi)^2 - 4m_e m_\chi^4]}{3m_\chi^4 (2E_R m_e + m_A^2)^2}. \quad \text{(A22)}$$

References

1. Young, B.L. A survey of dark matter and related topics in cosmology. *Front. Phys.* **2017**, *12*, 121201. Erratum in *Front. Phys.* **2017**, *12*, 121202. [CrossRef]
2. Fan, J.; Reece, M.; Wang, L.T. Non-relativistic effective theory of dark matter direct detection. *JCAP* **2010**, *11*, 042. [CrossRef]
3. Agrawal, P.; Chacko, Z.; Kilic, C.; Mishra, R.K. A Classification of Dark Matter Candidates with Primarily Spin-Dependent Interactions with Matter. *arXiv* **2010**, arXiv:1003.1912.
4. Freytsis, M.; Ligeti, Z. On dark matter models with uniquely spin-dependent detection possibilities. *Phys. Rev. D* **2011**, *83*, 115009. [CrossRef]
5. Fitzpatrick, A.L.; Haxton, W.; Katz, E.; Lubbers, N.; Xu, Y. Model Independent Direct Detection Analyses. *arXiv* **2012**, arXiv:1211.2818.
6. Han, T.; Kling, F.; Su, S.; Wu, Y. Unblinding the dark matter blind spots. *JHEP* **2017**, *2*, 57. [CrossRef]
7. Abdughani, M.; Wu, L.; Yang, J.M. Status and prospects of light bino–higgsino dark matter in natural SUSY. *Eur. Phys. J. C* **2018**, *78*, 4. [CrossRef]
8. Wang, W.; Yang, W.N.; Zhu, B. The Spin-dependent Scattering of Boosted Dark Matter. *arXiv* **2021**, arXiv:2111.04000.
9. Beacom, J. The End is Near for Testing Spin-Dependent Dark Matter. In Proceedings of the Aps Meeting, Baltimore, MD, USA, 14–18 March 2016.
10. Ramani, H.; Woolley, G. Spin-Dependent Light Dark Matter Constraints from Mediators. *arXiv* **2019**, arXiv:1905.04319.
11. Liu, C.P.; Wu, C.P.; Chen, J.W.; Chi, H.C.; Pandey, M.K.; Singh, L.; Wong, H.T. Spin-dependent dark matter-electron interactions. *arXiv* **2021**, arXiv:2106.16214.
12. Dodelson, S. *Modern Cosmology*; Academic Press: Amsterdam, The Netherlands, 2003.
13. Knapen, S.; Lin, T.; Zurek, K.M. Light Dark Matter: Models and Constraints. *Phys. Rev. D* **2017**, *96*, 115021. [CrossRef]
14. Essig, R.; Mardon, J.; Volansky, T. Direct Detection of Sub-GeV Dark Matter. *Phys. Rev. D* **2012**, *85*, 76007. [CrossRef]
15. Essig, R.; Fernandez-Serra, M.; Mardon, J.; Soto, A.; Volansky, T.; Yu, T.T. Direct Detection of sub-GeV Dark Matter with Semiconductor Targets. *JHEP* **2016**, *5*, 46. [CrossRef]
16. Athron, P.; Balázs, C.; Beniwal, A.; Camargo-Molina, J.E.; Fowlie, A.; Gonzalo, T.E.; Hoof, S.; Kahlhoefer, F.; Marsh, D.J.E.; Prim, M.T.; et al. Global fits of axion-like particles to XENON1T and astrophysical data. *JHEP* **2021**, *5*, 159. [CrossRef]
17. Gao, C.; Liu, J.; Wang, L.T.; Wang, X.P.; Xue, W.; Zhong, Y.M. Reexamining the Solar Axion Explanation for the XENON1T Excess. *Phys. Rev. Lett.* **2020**, *125*, 131806. [CrossRef] [PubMed]
18. An, H.; Pospelov, M.; Pradler, J.; Ritz, A. New limits on dark photons from solar emission and keV scale dark matter. *Phys. Rev. D* **2020**, *102*, 115022. [CrossRef]
19. Ge, S.F.; Pasquini, P.; Sheng, J. Solar neutrino scattering with electron into massive sterile neutrino. *Phys. Lett. B* **2020**, *810*, 135787. [CrossRef]
20. Du, M.; Liang, J.; Liu, Z.; Tran, V.Q.; Xue, Y. On-shell mediator dark matter models and the Xenon1T excess. *Chin. Phys. C* **2021**, *45*, 13114. [CrossRef]
21. Choi, S.M.; Lee, H.M.; Zhu, B. Exothermic dark mesons in light of electron recoil excess at XENON1T. *JHEP* **2021**, *4*, 251. [CrossRef]
22. Bloch, I.M.; Caputo, A.; Essig, R.; Redigolo, D.; Sholapurkar, M.; Volansky, T. Exploring new physics with O(keV) electron recoils in direct detection experiments. *JHEP* **2021**, *1*, 178. [CrossRef]
23. Knapen, S.; Kozaczuk, J.; Lin, T. Dark matter-electron scattering in dielectrics. *Phys. Rev. D* **2021**, *104*, 015031. [CrossRef]
24. Chao, W.; Jin, M.; Peng, Y.Q. Direct detection of Sub-GeV Dark Matter via 3-body Inelastic Scattering Process. *arXiv* **2021**, arXiv:2109.14944.
25. Hochberg, Y.; Kahn, Y.; Kurinsky, N.; Lehmann, B.V.; Yu, T.C.; Berggren, K.K. Determining Dark-Matter–Electron Scattering Rates from the Dielectric Function. *Phys. Rev. Lett.* **2021**, *127*, 151802. [CrossRef] [PubMed]
26. Essig, R.; Manalaysay, A.; Mardon, J.; Sorensen, P.; Volansky, T. First Direct Detection Limits on sub-GeV Dark Matter from XENON10. *Phys. Rev. Lett.* **2012**, *109*, 021301. [CrossRef] [PubMed]
27. Essig, R.; Volansky, T.; Yu, T.T. New Constraints and Prospects for sub-GeV Dark Matter Scattering off Electrons in Xenon. *Phys. Rev. D* **2017**, *96*, 043017. [CrossRef]
28. Dolan, M.J.; Kahlhoefer, F.; McCabe, C. Directly detecting sub-GeV dark matter with electrons from nuclear scattering. *Phys. Rev. Lett.* **2018**, *121*, 101801. [CrossRef]
29. Baxter, D.; Kahn, Y.; Krnjaic, G. Electron Ionization via Dark Matter-Electron Scattering and the Migdal Effect. *Phys. Rev. D* **2020**, *101*, 076014. [CrossRef]
30. Su, L.; Wang, W.; Wu, L.; Yang, J.M.; Zhu, B. Atmospheric Dark Matter and Xenon1T Excess. *Phys. Rev. D* **2020**, *102*, 115028. [CrossRef]
31. Lasenby, R.; Prabhu, A. DM-electron scattering in materials: sum rules and heterostructures. *arXiv* **2021**, arXiv:2110.01587.

32. Aprile, E.; Arisaka, K.; Arneodo, F.; Askin, A.; Baudis, L.; Behrens, A.; Brown, E.; Cardoso, J.M.R.; Choi, B.; Cline, D.; et al. The XENON100 Dark Matter Experiment. *Astropart. Phys.* **2012**, *35*, 573–590. [CrossRef]
33. Aprile, E.; Alfonsi, M.; Arisaka, K.; Arneodo, F.; Balan, C.; Baudis, L.; Bauermeister, B.; Behrens, A.; Beltrame, P.; Bokeloh, K.; et al. Limits on spin-dependent WIMP-nucleon cross sections from 225 live days of XENON100 data. *Phys. Rev. Lett.* **2013**, *111*, 021301. [CrossRef] [PubMed]
34. Aprile, E.; Aalbers, J.; Agostini, F.; Alfonsi, M.; Amaro, F.D.; Anthony, M.; Arneodo, F.; Barrow, P.; Baudis, L.; Bauermeister, B.; et al. Low-mass dark matter search using ionization signals in XENON100. *Phys. Rev. D* **2016**, *94*, 092001. Erratum in *Phys. Rev. D* **2017**, *95*, 059901. [CrossRef]
35. Aprile, E.; Aalbers, J.; Agostini, F.; Alfonsi, M.; Althueser, L.; Amaro, F.D.; Antochi, V. C.; Angelino, E.; Arneodo, F.; Barge, D.; et al. Light Dark Matter Search with Ionization Signals in XENON1T. *Phys. Rev. Lett.* **2019**, *123*, 251801. [CrossRef] [PubMed]
36. Engel, J.; Pittel, S.; Vogel, P. Nuclear physics of dark matter detection. *Int. J. Mod. Phys. E* **1992**, *1*, 1–37. [CrossRef]
37. Clark, B.C.; Hama, S.; Mercer, R.L.; Ray, L.; Serot, B.D. Dirac-Equation Impulse Approximation for Intermediate-Energy Nucleon-Nucleus Scattering. *Phys. Rev. Lett.* **1983**, *50*, 1644–1647. [CrossRef]
38. Forest, T.D. Off-shell electron-nucleon cross sections: The impulse approximation. *Nucl. Phys. A* **1983**, *392*, 232–248. [CrossRef]
39. Campbell-Deem, B.; Knapen, S.; Lin, T.; Villarama, E. Dark matter direct detection from the single phonon to the nuclear recoil regime. *arXiv* **2022**, arXiv:2205.02250.
40. Catena, R.; Emken, T.; Spaldin, N.A.; Tarantino, W. Atomic responses to general dark matter-electron interactions. *Phys. Rev. Res.* **2020**, *2*, 033195. [CrossRef]
41. Griffin, S.M.; Inzani, K.; Trickle, T.; Zhang, Z.; Zurek, K.M. Extended calculation of dark matter-electron scattering in crystal targets. *Phys. Rev. D* **2021**, *104*, 095015. [CrossRef]
42. Pandey, M.K.; Singh, L.; Wu, C.P.; Chen, J.W.; Chi, H.C.; Hsieh, C.C.; Liu, C.P.; Wong, H.T. Constraints from a many-body method on spin-independent dark matter scattering off electrons using data from germanium and xenon detectors. *Phys. Rev. D* **2020**, *102*, 123025. [CrossRef]
43. Chen, J.W.; Chi, H.C.; Liu, C.P.; Wu, C.L.; Wu, C.P. Electronic and nuclear contributions in sub-GeV dark matter scattering: A case study with hydrogen. *Phys. Rev. D* **2015**, *92*, 096013. [CrossRef]
44. Smith, M.C.; Ruchti, G.R.; Helmi, A.; Wyse, R.F.G.; Fulbright, J.P.; Freeman, K.C.; Navarro, J.F.; Seabroke, G.M.; Steinmetz, M.; Williams, M.; et al. The RAVE Survey: Constraining the Local Galactic Escape Speed. *Mon. Not. Roy. Astron. Soc.* **2007**, *379*, 755–772. [CrossRef]
45. Dehnen, W.; Binney, J. Local stellar kinematics from hipparcos data. *Mon. Not. Roy. Astron. Soc.* **1998**, *298*, 387–394. [CrossRef]
46. Feldstein, B.; Fitzpatrick, A.L.; Katz, E. Form Factor Dark Matter. *JCAP* **2010**, *1*, 20. [CrossRef]
47. Cao, Q.H.; Ding, R.; Xiang, Q.F. Searching for sub-MeV boosted dark matter from xenon electron direct detection. *Chin. Phys. C* **2021**, *45*, 45002. [CrossRef]